Three-dimensional organisation of re-entrant propagation during experimental ventricular fibrilation

V.N. Biktashev[1,2,3], A.V. Holden [3],
S.F. Mironov[4], A.M. Pertsov[4] and A.V. Zaitsev[4]

July 30, 2001

[1]Department of Mathematical Sciences, University of Liverpool, Liverpool L69 7ZL, UK
[2]On leave from: Institute for Mathematical Problems in Biology, Pushchino, 142292, Russia
[3]School of Biomedical Sciences, University of Leeds, Leeds LS2 9JT, UK
[4]Department of Pharmacology, SUNY Health Science Center, 750 East Adams St., Syracuse, NY 13210, USA

Abstract

Ventricular fibrillation is believed to be produced by the breakdown of re-entrant propagation waves of excitation into multiple re-entrant sources. These re-entrant waves may be idealised as spiral waves in two dimensional, and scroll waves in three dimensional excitable media. Optically monitored, simultaneously recorded endocardial and epicardial patterns of activation on the ventricular wall not always show spiral waves. Analysis of optically recorded irregular electrical wave activity on the surface of the heart during experimentally induced fibrillation reveals a strong local temporal periodicity. The spatial distribution of the dominant temporal frequencies of excitation has a domain organization. The domains are large ($\approx 1\,\mathrm{cm}^2$) and they persist for minutes. We show that numerical simulations, even with a simple homogeneous excitable medium, can reproduce the key features of the simultaneous endo- and epicardial visualisations of propagating activity, and so these recordings may be interpreted in terms of scroll waves within the ventricular wall.

The domain structure can be reproduced in a two-dimensional excitable medium governed by the FitzHugh-Nagumo equations with a spatial inhomogeneity. We identified two potential mechanisms that may contribute to the observed experimental dynamics: coexistence of stable spiral waves with non-commensurate frequencies of rotation, and Wenckebach-like frequency division from a single spiral source due to inhomogeneity. Both mechanisms reproduce the uniformity of the dominant frequency within individual domains and sharp boundaries between domains. The possibility of distinguishing between different mechanisms using Lissajous figures is discussed.

1 Introduction

Ventricular fibrillation almost invariably occurs during the process of dying, and its onset underlies sudden cardiac death. It is widely believed that the mechanism of ventricular fibrillation is that it is produced by one or many re-entrant (spiral in 2D or scroll in 3D) propagating waves of excitation in the ventricular wall — see [1] [2], [3], [4] and [5] for numerical experiments with scroll waves in anatomically accurate models.

Recently, detailed mapping of the surface electrical activity of the heart has become possible [6, 7]. The patterns of excitation during experimental fibrillation may show no spiral waves on either surface of the heart muscle. This difference between theory and experiment may mean either that the fibrillation is not due to re-entry, or that the re-entry waves are masked by the inhomogeneity, anisotropy and three-dimensional nature of the ventricular wall. Quantitative analysis of the excitation patterns has led to the observation that the dominant frequency of oscillations has a domain structure, the dominant frequency being approximately uniform within one domain but different in different domains, and the boundaries between the domains being quite sharp, with the domains persisting over tens of seconds *i.e.* hundreds of times longer than the approximate periodicity of the local oscillations [8, 9]. Here we show that the three-dimensional nature of the wall alone is enough to qualitatively explain the experimental observations, as these observations can be reproduced in numerical experiments with a simple mathematical model.

Mathematical models of cardiac excitability based on voltage clamp experiments with single cardiac cells and single channels use many variables to describe each cell, and can take into account the bidomain and anisotropic nature of the cell-to-cell conductivity and tissue inhomogeneity:

$$\begin{aligned} \partial_t E &= F(E, g_j, \vec{r}) + \hat{\mathcal{D}} \cdot E, \\ \partial_t g_i &= G_i(E, g_j, \vec{r}), \\ i, j &= 1, \ldots, N, \end{aligned}$$

where $\vec{r}$ is a vector of spatial coordinates; E is the transmembrane voltage; $\hat{\mathcal{D}}$ is the conductivity operator, which may explicitly depend on $\vec{r}$ and is integro-differential to take into account the bidomain structure of the tissue or degenerates into a Laplacian if it does not; and $g = (g_1, g_2 \ldots)^{\mathrm{T}}$ is a column-vector of local variables, including gating variables and ionic concentrations. In the case of the OXSOFT model of guinea-pig ventricular cell [10, 11], $N = 16$. An illustration of re-entrant activity obtained in such a model is shown on Fig. $1(a)$, where we have used a second-order differential operator for conductivity suggested by Panfilov and Keener [12] and Fenton and Karma [13]:

$$\hat{\mathcal{D}} \cdot E = \sum_{i,j=1}^{3} \frac{\partial}{\partial r_i} D_{i,j}(\vec{r}) \frac{\partial E}{\partial r_j}. \tag{1}$$

This form takes into account the rotational anisotropy of the real ventricular tissue: the direction of the fibres which is the direction of the largest eigenvector of the conductivity

tensor $D_{i,j}$. This is a scroll wave in a small ($5 \times 5 \times 1.5$ mm) slab of tissue with specially chosen boundary conditions, to permit the existence of a re-entrant wave (with zero-flux boundary conditions, a persistent re-entry wave in this model requires a larger piece of ventricular wall).

The complicated local kinetics and complicated description of conductivity makes such a biophysically detailed virtual cardiac tussue computationally expensive. Some qualitative results can be obtained for simpler models, which caricature the excitation and propagation properties of cardiac tissue. Neither complicated and stiff local kinetics, nor inhomogeneity or anisotropy are required to produce complicated spatio-temporal behaviour of the excitable medium. We used for simulations the simple homogeneous FitzHugh-Nagumo ($N = 1$) excitable medium model with simple diffusion-like conductivity. At some parameter values, the scroll wave filaments in this model have negative tension, which leads to their breakup and development of a three-dimensional "turbulence" of excitation waves, resembling fibrillation [14, 15]. Figure 1(b) shows a scroll wave in this model before the breakup into two pieces. The surface patterns of this "numerical fibrillation" demonstrate the same qualitative features as the patterns observed in optical mapping experiments.

We explore possible mechanisms of the domain structure. Our basic assumption is that fibrillation is caused by pinned re-entrant vortices[16, 9]. As a single spiral wave would only produce a periodic (monomorphic) pattern, some modification is required to explain the polymorphic behaviour. We consider two hypothesis:

M: There are two (or more) different re-entry vortices with different periods, and the domains of influence of the vortices are the dominant frequency domains.

W: There is essentially only one re-entry vortex, but its period is shorter than the minimal propagation period in some parts of the tissue, so in those parts intermittent conduction causing simple rational frequency division is observed. In cardiology this is described as Wenckebach frequency division.

Note that the hypothesis M is not quite trivial. It is a widespread belief that two or more periodic sources of waves in an excitable medium cannot coexist for a long time, as the fastest source should entrain all others. The mechanism of such entrainment is based on the observation that the excitation waves, in the head-on collisions, annihilate in the ratio 1:1. This sometimes leads to a natural but hastily drawn conclusion that coexistence of sources of different frequencies in the same medium is impossible [17]. Entrainment by the fastest source, however, assumes a relative homogeneity of the medium. If the medium is strongly nonhomogeneous, then it is conceivable that the waves of the faster source may be simply unable to penetrate the more refractory part of the medium where the slower source is located. As a result, some excitation waves annihilate by themselves without colliding with other waves, and no entrainment will occur. Note that different frequencies of spiral waves imply an inhomogeneity of properties, in particular the refractoriness.

Using simulations, we identify the key features of the excitation patterns corresponding to each of the two mechanisms, and apply this to the patterns observed in the isolated

tissue experiments. The result is that both hypotheses are consistent with the experimental data. Moreover, both mechanisms may be involved, either simultaneously, or one mechanism may switch to the other. In all cases a small number of re-entrant sources in an inhomogeneous medium is sufficient to reproduce the characteristics of the experimentally observed domains.

2 Methods

Numerical For homogeneous, three dimensional tissue we used for simulations the FitzHugh-Nagumo system of equations:

$$\begin{aligned} \partial_t u &= \epsilon^{-1}(u - u^3/3 - v) + \nabla^2 u, \\ \partial_t v &= \epsilon(u + \gamma - \beta v), \end{aligned} \tag{2}$$

where $\epsilon = 0.3$, $\beta = 0.75$ and $\gamma = 0.5$, with forward-time Euler differencing with time step 0.03 t.u. and simplest seven-point approximation of the Laplacian on a rectangular grid with space step 0.5 s.u., in media of different size with non-flux boundary conditions. The period of spiral wave in this model is about 20 t.u., This choice of parameters provides negative tension of the filaments, *i.e.* scroll waves in sufficiently large media are unstable, their filaments tend to lengthen, curve, touch the boundaries and each other and break onto pieces, each of which then grows again etc. At the same time, the same set of equations in two spatial dimensions shows quite stable spiral waves. This is in qualitative correspondence with the fact that real fibrillation is only observed in sufficiently thick hearts or heart preparations. The activation patterns at the opposite (upper and lower) surfaces of the medium were recorded and visualised in the same way as experimental patterns.

Both hypotheses for the domain structure require a macroscopic inhomogeneity of the tissue. It is well known that in an inhomogeneous medium re-entrant vortices tend to drift [18, 19, 20]. To prevent this drift and so produce numerical simulations of stationary rotating vortices in an inhomogeneous medium, we exploited the effect of pinning to localised inhomogeneities [21, 22, 17]. We used the following inhomogeneous variant of the FitzHugh-Nagumo system:

$$\begin{aligned} \frac{\partial u}{\partial t} &= \epsilon_u^{-1}(\mathbf{r})(u - u^3/3 - v) + \nabla^2 u \\ \frac{\partial v}{\partial t} &= \epsilon_v(\mathbf{r})(u + \beta - \gamma v), \end{aligned} \tag{3}$$

in a rectangular region $\mathbf{r} \in [0, X] \times [0, Y]$, $X = 30$, $Y = 12$, with impermeable boundaries, for $\beta = 0.68$ and $\gamma = 0.5$. Parameters $\epsilon_{u,v}$ depended on $\mathbf{r}$, to represent spatial

inhomogeneities (see Fig. 2):

$$\begin{aligned}
\epsilon_v(\mathbf{r}) &= \epsilon/\chi(\mathbf{r}), \\
\epsilon_u(\mathbf{r}) &= \epsilon\chi(\mathbf{r})\left(1 + K\exp\{-|(\mathbf{r}-\mathbf{r}_l)/\lambda_l|^2\} + K\exp\{-|(\mathbf{r}-\mathbf{r}_r)/\lambda_r|^2\}\right), \\
\chi(\mathbf{r}) &= = 1 + \frac{1}{2}\left(1 + \tanh\left(\frac{x - x_b}{w}\right)\right)(k-1).
\end{aligned} \tag{4}$$

The function $\chi(\mathbf{r})$ provided a macroscopical inhomogeneity, namely, a non-specific k-fold slowdown of all dynamic variables in the right hand part of the medium compared to the left, and the terms $K\exp()$ in ϵ_u provided a localised suppression of excitability in two 'holes', the regions with radii of the order λ_l. Figure 2 illustrates the distribution of ϵ_u and ϵ_v in the medium, for two different parameter sets used in the numerics. These sets were different in parameters k and w: $k = (1+\sqrt{5})/2 \approx 1.618$ and $w = 3$ (producing a stronger but smoother inhomogeneity) and $k = \sqrt{2} \approx 1.414$ and $w = 0$ (producing a slighter but sharper, stepwise inhomogeneity). Other parameters were $\epsilon = 0.3$, $K = 100$, $\lambda_l = 0.6$, $\lambda_r = \lambda_l\sqrt{k}$, $\mathbf{r}_l = (0.15X, 0.5Y)$, $\mathbf{r}_r = (0.8X, 0.5Y)$, and $x_b = 0.4X$.

The initial conditions were established as follows. A spiral wave was initiated in a homogeneous medium ($k = 1$, $K = 0$). The dynamic variables $U(\phi) = u(\mathbf{r}, 2\pi t/T)$, $V(\phi) = v(\mathbf{r}, 2\pi t/T)$ were recorded at a point $\mathbf{r}$ far from the core of the spiral, for one rotation period, $t \in [0, T]$. This recording was used to create initial conditions for the inhomogeneous medium, $u(\mathbf{r}, 0) = U(\phi)$, $v(\mathbf{r}, 0) = V(\phi)$, where the distribution of the phase ϕ was specified to provide either one spiral wave,

$$\phi = |\mathbf{r} - \mathbf{r}_l|/\Lambda_l - \arg(\mathbf{r} - \mathbf{r}_l), \tag{5}$$

or two spiral waves,

$$\phi = \max\left\{|\mathbf{r} - \mathbf{r}_l|/\Lambda_l - \arg(\mathbf{r} - \mathbf{r}_l), -|\mathbf{r} - \mathbf{r}_r|/\Lambda_r + \arg(\mathbf{r} - \mathbf{r}_r)\right\}, \tag{6}$$

around the inexcitable holes $\mathbf{r}_l$, $\mathbf{r}_r$. Here $\Lambda_l = 3$, $\Lambda_r = \Lambda_l\sqrt{k}$, and $\arg(\mathbf{r})$ is defined as the angle made by vector $\mathbf{r}$ with the x-axis (counter-clockwise being positive).

Simulations were performed with spatial step 0.2 space units (s.u.) of (3) and output data were sampled with interval 0.64 time units of (3). The value of the variable u in the solutions to (3) was taken as an equivalent of the optical signal in the experimental procedure described below. The time unit of (3) was assumed to correspond to 13 ms., as if the numerical data were sampled with the frequency 120 Hz; this provides a rough correspondence of the oscillations frequencies observed in experiment and in numerics.

Experimental Experimental visualisations of electrical activity were from the endo- and epicardial surfaces of pieces of sheep ventricular wall (5-11 mm thick) that had been excised and perfused via the coronary arteries, and superfused with oxygenated physiological saline containing a drug (diacetyl monoxime), that blocked contraction, and a potential-sensitive dye (di-4-ANEPPS). The video images were obtained at 120 frames/s with a spatial resolution of approximately 0.5 mm . The optical signals at different points were normalised

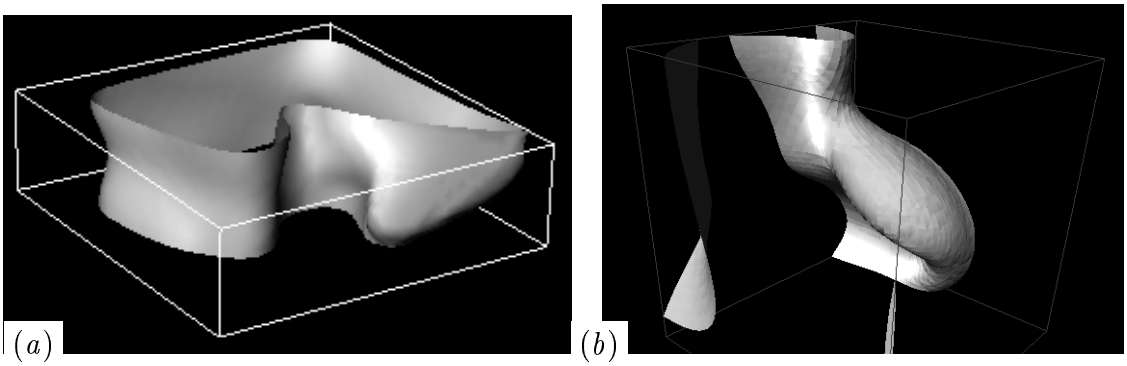

Figure 1: Scroll waves in mathematical models of excitable tissues. (a) Kinetics of OXSOFT guinea-pig ventricular cell, with rotational anisotropy of conductivity tensor. (b) FitzHugh-Nagumo model with homogeneous isotropic conductivity, but with negative tension of scroll filaments. Shown are the isosurfaces of the excitation variable.

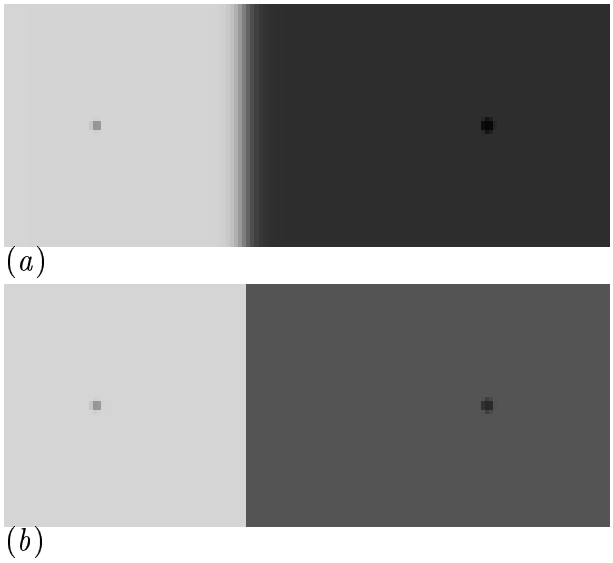

Figure 2: Spatial distribution of the parameter ϵ_v in numerical experiments. Lighter shade represents higher value of ϵ_v. (a) Smooth inhomogeneity, $k \approx 1.618$, $w = 3$. (b) Weaker and sharp, stepwise inhomogeneity, $k \approx 1.414$, $w = 0$. Two localised defects shown as the dark spots are regions of reduced excitability, *i.e.* high value of ϵ_u.

to allow for the variations of the dye concentration etc. The points where the signal was too low were excluded from consideration, so the shape of the patterns represents not the excitable ventricular preparation, but merely the stained part of it, typically of the size of about $3 \times 3\,\mathrm{cm}^2$. More technical details can be found in [23].

Irregular, self-sustained re-entrant propagation can be induced in a resting tissue preparation by rapid electric pacing; this provides an experimental model for the electrical activity during ventricular tachycardia (high — up to about 10 Hz— frequency activity, believed to be due to simple re-entry in the ventricle) and fibrillation (irregular, high frequency activity due to multiple re-entrant sources). Figure 3 shows typical images of endocardial activity.

Periods of excitation in our experiments were up to about 200 ms in "monomorphic tachycardia" and in the range of 100–150 ms in "fibrillation". So we may scale the time unit of (3) roughly as 5–10 ms.

Visualisation The volume patterns (Fig. 4(c) and Fig. 5(c)) were visualised analogously to Fig. 1, using isosurfaces of E, namely $E = 0$. To reveal more details of the complicated spatial structures, we showed only wavefronts (lower values of g, semi-transparent), and their edges (intermediate values of g, non-transparent), and made the wavebacks (higher values of g) invisible.

2.1 Data processing

The processing included calculation of pseudo-ECG, and finding pointwise Fourier spectra with subsequent pointwise bandpass filtering of the signals and calculating the spatial distribution of powers of the frequency bands.

Pseudo-ECG The pseudo-ECG signals were calculated from the experimental and simulation data, $u(x, y, t)$, by simple summation,

$$E(t) = \iint u(x, y, t)\,\mathrm{d}x\mathrm{d}y. \tag{7}$$

Both the real ECG and the calculated $E(t)$ are integral characteristics of electrical activity; $E(t)$ has an advantage that it can be easily obtained directly from optical mapping data, and from the results of numerical simulations, thus providing a uniform approach to both types of datasets.

Fourier spectra We performed a pointwise discrete Fourier transform on both the simulation and tissue experimental data,

$$\tilde{u}(x, y, f) = \mathcal{F}[u(x, y, t)] \tag{8}$$

to obtain the cumulative power spectra,

$$P(f) = \iint |\tilde{u}(x, y, f)|^2 \, \mathrm{d}x \, \mathrm{d}y. \tag{9}$$

Note that a cumulative power spectrum obtained by (9) is a spectrum of the whole signal, *not* a power spectrum of the pseudo-ECG (7).

Filtering Given the frequencies of the main peaks and peak widths, the signals were then filtered to one of the two or three windows,

$$W_j(f) = \exp\left(-Q_j(1 - f/f_j)^4\right), \tag{10}$$

where f_j, $j = 1, 2(, 3)$ are the central frequencies of the windows, and Q_j are coefficients representing filtering quality. Parameters f_j and Q_j were chosen based on the visual analysis of frequency spectra of the experimental or numerical data, so that each window is reasonably wide but covers only one frequency peak.

Frequency band power distributions The distribution of the power of the frequency band j was computed as

$$B_j(x, y) = \int |\tilde{u}(x, y, f)|^2 W_j(f) \, \mathrm{d}f \tag{11}$$

and these distributions were then visualised as density plots, with black corresponding to zero and white to the maximal value of $B_j(x, y)$.

3 Results

In experimentally observed patterns of surface actiity, most often, no spiral waves are apparent and the activity appears to be irregular in space, while at any point it is repetitive (roughly periodic) in time. The apparent complexity of the patterns of activity on the heart surface does not remain the same during an episode of experimental ventricular fibrillation, and this does not appear to be by spiral waves breaking down into irregularity. Cores of spiral waves are shown in the pictures by symbols ⊛ and ⊛. The locations of these cores were done manually by visuial analysis of the movies rather than still pictures. Though the automatic detection of phase singularities is possible [6], manual detection is more reliable. Figure 3 shows two snapshots from the same experiment. In less than three seconds, the propagation pattern has changed completely, and where a spiral wave was at one moment, plane waves are seen later.

The typical qualitative properties of experimentally observed excitation patterns can be summarised as follows.

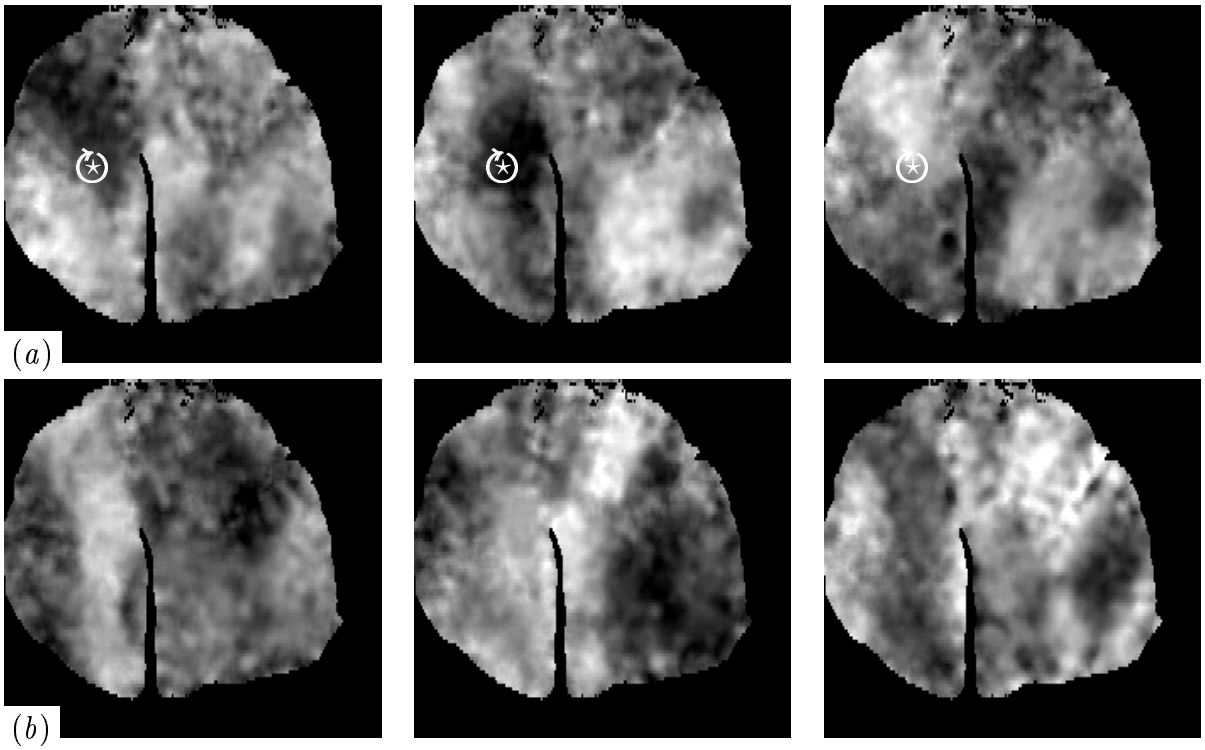

Figure 3: Transient spiral wave on the epicardial surface. Shown are experimental frames with the interval 25ms. (a) Spiral wave rotates clockwise, symbol ⟲ shows the rotation center. (b) The same preparation, 2.5 s later. No spiral wave is seen; the activation pattern is nearly plane waves propagating from left to right. The dark line is the "shadow" of an electrode.

- Synchronous endo- and epicardial views of the same preparation can, and most often do, show different dynamics. In case of simple excitation pattern, corresponding to monomorphic tachycardia, the patterns are different but synchronous; in more complex cases, corresponding to polymorphic tachycardia/fibrillation, they seem virtually independent.

- At every particular point, most of the time the electrical activity is approximately periodic. The spatio-temporal pattern as a whole can be approximately periodic, in the examples that correspond to monomorphic tachycardia, but not in the examples that correspond to polymorphic tachycardia/fibrillation.

- During fibrillation, spiral waves are sometimes seen on the surfaces, but quite often they are not. If they are seen, they appear only transiently, for a few rotations, and then disappear.

- The (visual) complexity of the patterns changes with time; at large times, it appears to increase.

All these observations are consistent with scroll waves of excitation within the bulk of the ventricular wall. We illustrate this by numerical simulations. Mathematical models can be used to reconstruct the excitation patterns on the surface and within the bulk of the tissue, while with current experimental techniques only the surface patterns can be directly visualised. Simulating this model in different medium sizes, we were able to reproduce the qualitative features of the experimental surface patterns. Two typical examples are shown on Fig. 4 and Fig. 5.

Figure 4(a) shows activity in which the epicardial surface is being depolarised by an almost spatially uniform, time periodic depolarisation, while activity on the endocardial surface is a wave train propagating from left to right. In both cases the temporal period is approximately 190 ms. A simple three dimensional mechanism for this would be a single scroll wave, with its filament roughly parallel to the surfaces of the heart, and its position closer to the endocardial surface, as illustrated by Fig. 4(b,c). If the filament were far from the epicardial surface, the excitation wavefront would meet the epicardial surface almost simultaneously, giving a spatially uniform depolarisation. If the filament were closer to the epicardial surface, the curved excitation wavefront would first meet the epicardial surface as a narrow band, and excitation would propagate perpendicular to the band, in both directions, at a velocity faster than the propagation velocity for a plane wave. This is seen in Fig. 4(c), where the apparent velocity of the simulated epicardial wave front is considerably higher than that of the endocardial wave, that has the same period. Krinsky et al [24] have suggested such a scroll wave, or scroll ring, as an explanatory mechanism for a narrow band of surface excitation that spreads away in both directions from its midline. For the model (2)), with the parameters used, a single scroll wave is unstable in a large medium[15], and so a double scroll is used to reproduce this behaviour in Fig. 4(b,c). On the nearest and on the most distant surfaces of the medium, two-armed spiral waves would be seen; but the activation patterns on the upper and lower surfaces do not show spiral

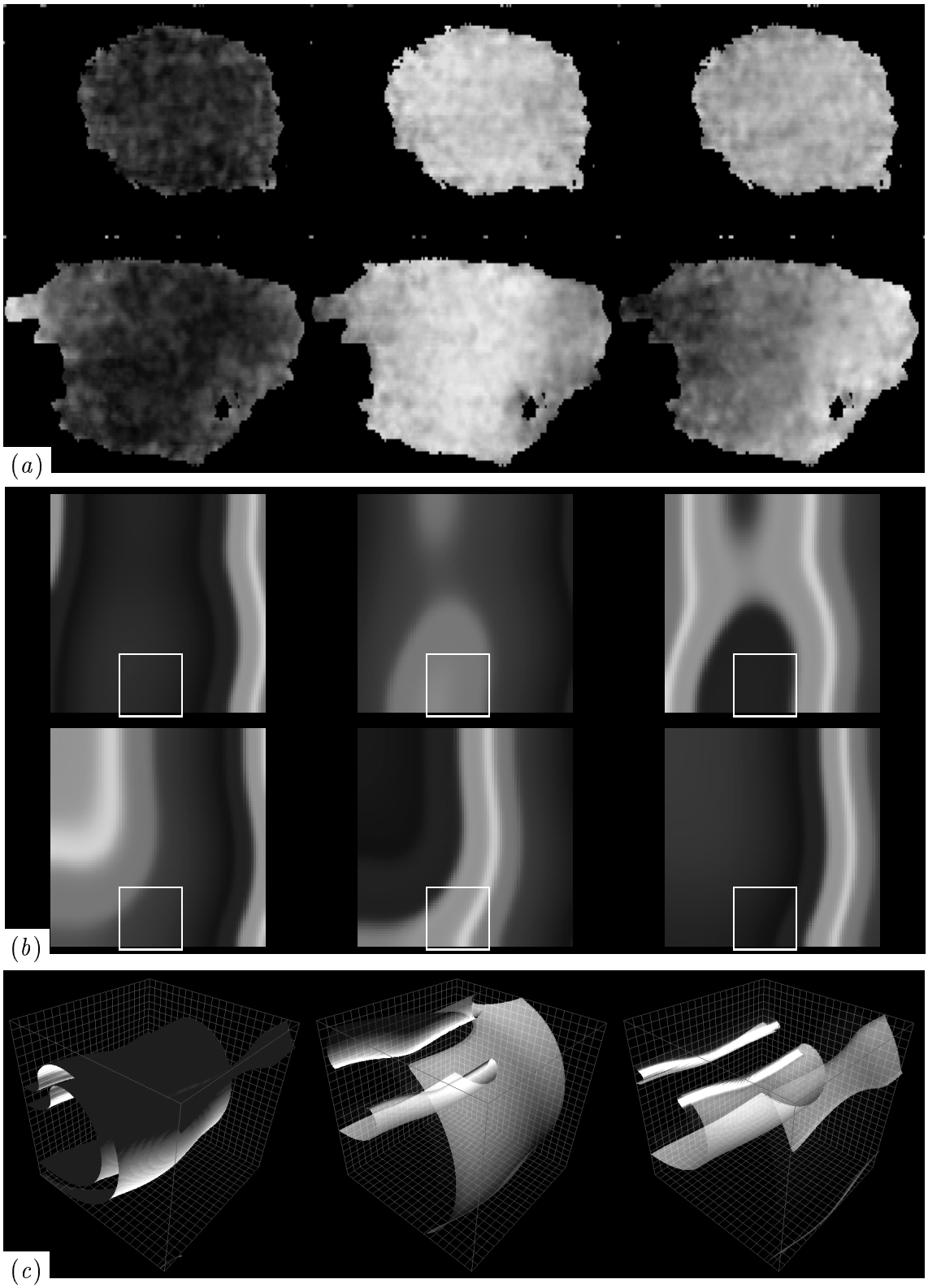

Figure 4: Comparison of experimental surface views of simple excitation pattern ("monomorphic tachycardia") with numerical simulations of metastable double scroll in FHN (medium size $43 \times 43 \times 43$ s.u.). (a) experimental patterns, the upper three pictures are epicardial views and the lower three pictures are endocardial views with interval 50 ms. (b): numerical simulations, surface patterns. White frames show the region where the behaviour in the experiment. (c): numerical simulations, corresponding volume view.

waves. The filaments of the double scroll are curved and far enough from the upper surface. Therefore, the front is convex when approaching this surface, and a focal source of waves is observed at the point where the wavefront first touches it. And the lower surface shows just waves propagating from left to right, as it is close to the double scroll filaments, and the emanated wave is not convex enough to form a focal source.

White frames on Fig. 4b indicate an area where the experimental excitation patterns of Fig. 4a are reproduced almost literally. Namely, synchronous oscillations on the epicardial surface, and waves from the top-left corner to the right-hand side, not the endocardial surface. That is, if only the region within this white frame was "stained" with the voltage-sensitive dye, we would see exactly the same activation pattern as in the real experiment.

The more complicated, irregular surface views are characteristic of the later, "fibrillation" stages. Such views can be qualitatively reproduced by a small number of interacting scrolls that are continually breaking down and being born from broken wavefronts. This is illustrated in Fig. 5, where the model parameters are such that simple (single or double) scroll waves are unstable and breakdown occurs. The endo- and epicardial images show coherence at the scale of the action potential wavelength, so can be described as propagating, curved wavefronts, that sometimes have ends (corresponding to a phase singularity), and occasionally spiral forms can be identified. The feature of these surface images can be simulated by a few interacting scroll waves. The "literal" reproduction of experimental patterns in the mathematical model seem to have little sense. The reason is that the dynamics of the scroll waves in this model is inherently unstable, analogously to the Kuramoto-Sivashinsky wavefronts, and arbitrarily small difference in initial conditions leads to significant difference in the solution [15]. This feature is essential for the imitation of the fibrillation, if the latter to be considered as a chaotic process. Figure 5 shows a typical experimental pattern and its rough qualitative analogue found in a numerical experiment. On the epicardial surface of the experiment and on the top surface in the model, there are two spiral waves, one rotating clockwise and the other counterclockwise. On the endocardial and bottom surfaces, the pattern is more complicated: one counterclockwise rotating spiral (close to the right edge of visible area of the experimental preparation, and close to the upper edge of the numerical picture), and two-armed clockwise spiral in the middle. The positions of single spiral waves in all cases were relatively stable, *i.e.* they remained on the same place for a few rotations or slowly drifted, both in experiment and in the model. The two-armed spirals showed significant meander, again, both in the experiment and in the model, so the double ⊛ symbols only very approximately show their location. Double spiral wave could be produced by an appropriately oriented double scroll analogous to that shown on Fig. 4(b). However, we can see from Fig. 5(c) that it was not the case here, and the two filament are close to each other only near the surface and are independent in the bulk; perhaps, this could be related to their strongly nonstationary behaviour. This suggests that the appearance of the double spiral *i.e.* of the two spirals of the same sign together, might be a transient and, in a sense, an accidental event, same as an appearance of a single spiral. This is different from the appearance of pairs of spirals of opposite signs as described in [6] which appear or annihilate on a regular basis as a result of a scroll filament touching the surface or detaching from from it.

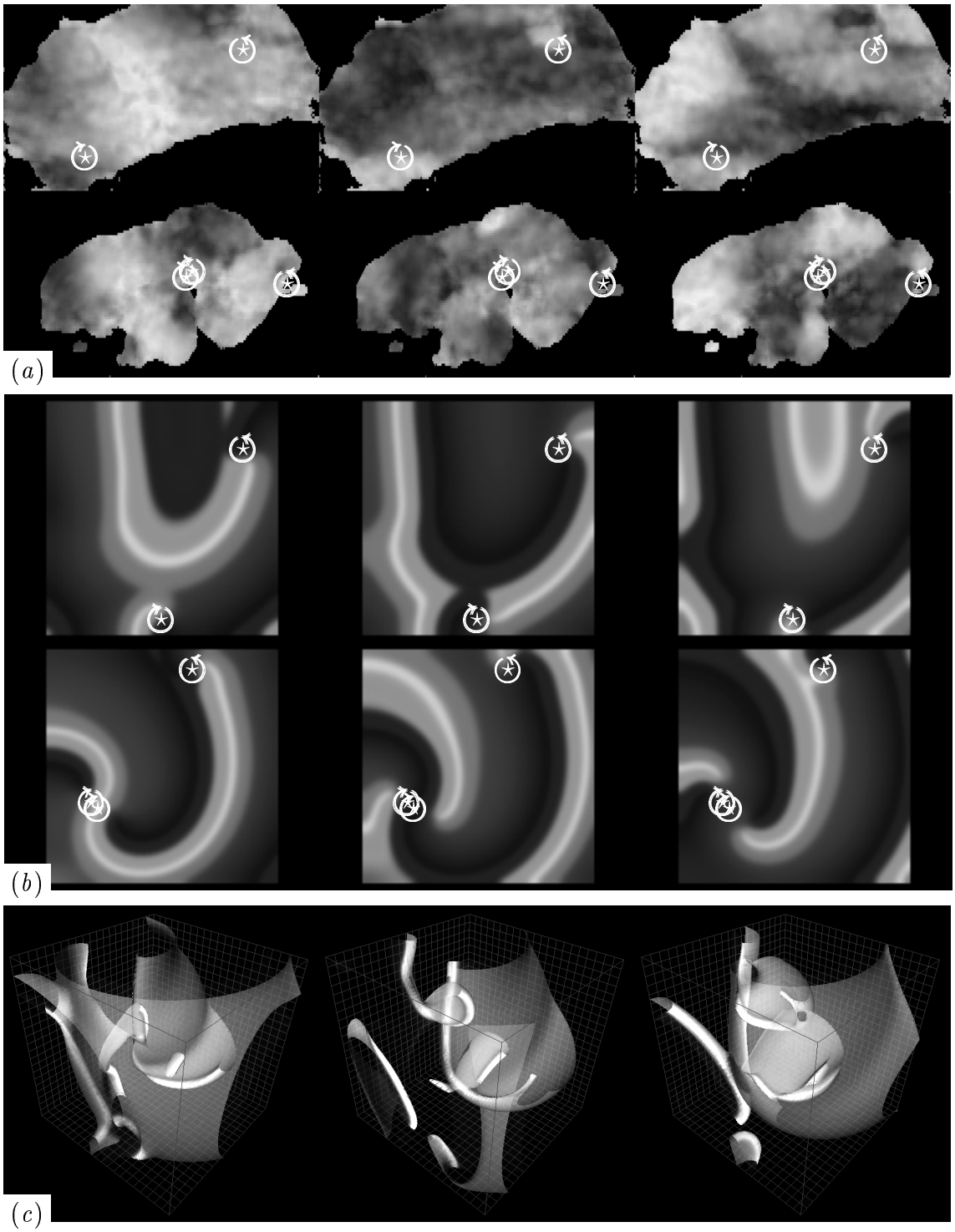

Figure 5: Comparison of experimental surface views of polymorphic tachycardia with numerical simulations of scroll turbulence in FHN (medium size $50 \times 50 \times 50$ s.u.). Layout is the same as on Fig. 4. The spiral waves are shown by white ⊛ and ⊛ symbols. Interval between experimental patterns 50 ms; between numerical patterns 4.2 t.u.

All qualitative features summarised above, are reproduced in the numerical model. Namely,

- The patterns on opposite surfaces are indeed different, which is an obvious consequence of the three dimensional nature of the model. Moreover, if multiple scrolls are present, the pictures are not only different, but look uncorrelated.

- The dynamics of scroll waves is approximately periodic rotation around the filaments which can slowly move. This provides local approximate periodicity almost everywhere. Filaments of multiple scroll waves do not remain in rest, which provides the absence of global periodicity. Only simple (single or double) scrolls contained in a small volume, or attached to medium boundary, showed no drift in this model, and in this case the surface patterns were approximately periodic as a whole.

- The mobility of the multiple scrolls makes it quite likely for the filaments to appear on a surface for a short time and then disappear again; this is seen on the surface as a transient spiral wave.

- The complexity of the volume behaviour and of the surface patterns increases with the size of the medium, and requires lowered excitability of the local kinetics. Both these factors are in correspondence with changes in electrophysiology of the cardiac tissue during fibrillation.

3.1 Frequency domains in experimental fibrillatory patterns

Figures 6 and 7 illustrate the frequency domain structure in experimental fibrillatory patterns.

On Figs. 6 and 7, the top two plots are the pseudo-ECG $E(t)$ and cumulative power spectrum $P(f)$. Experimental data demonstrated a smooth shape of the recorded action potential, which produced virtually no higher harmonics, and the main peaks were easily identifiable, though often partially overlapping, as in Fig. 6. The density plots are is the frequency domain maps: the spatial distribution of the frequency bands power over the preparation $B_j(x, y)$. The frequency windows $W_j(f)$ and power spectra of the whole preparation after bandpass filtering $P(f)W_j(f)$ are shown to the right of the domain maps. Lower panels show individual signals from different points of the preparation, together with their power spectra.

The pseudo-ECG signals show polymorphic or fibrillatory activity, especially Figs. 7 . Yet, the power spectra $P(f)$ clearly show two dominant frequencies for Figs. 6 and three for Fig. 7. The feature of the total power spectrum in Fig. 6 is that the two bands overlap, and so it is not obvious that they correspond to different processes. Yet, in all examples, on the frequency distribution $B_j(x, y)$ panel one can clearly see the large light regions appearing only on one of the density plots, as well as narrower regions which are light on two or three maps. The different frequencies of oscillations are spatially separated, in domains. This is confirmed by the analysis of time series recorded at different points.

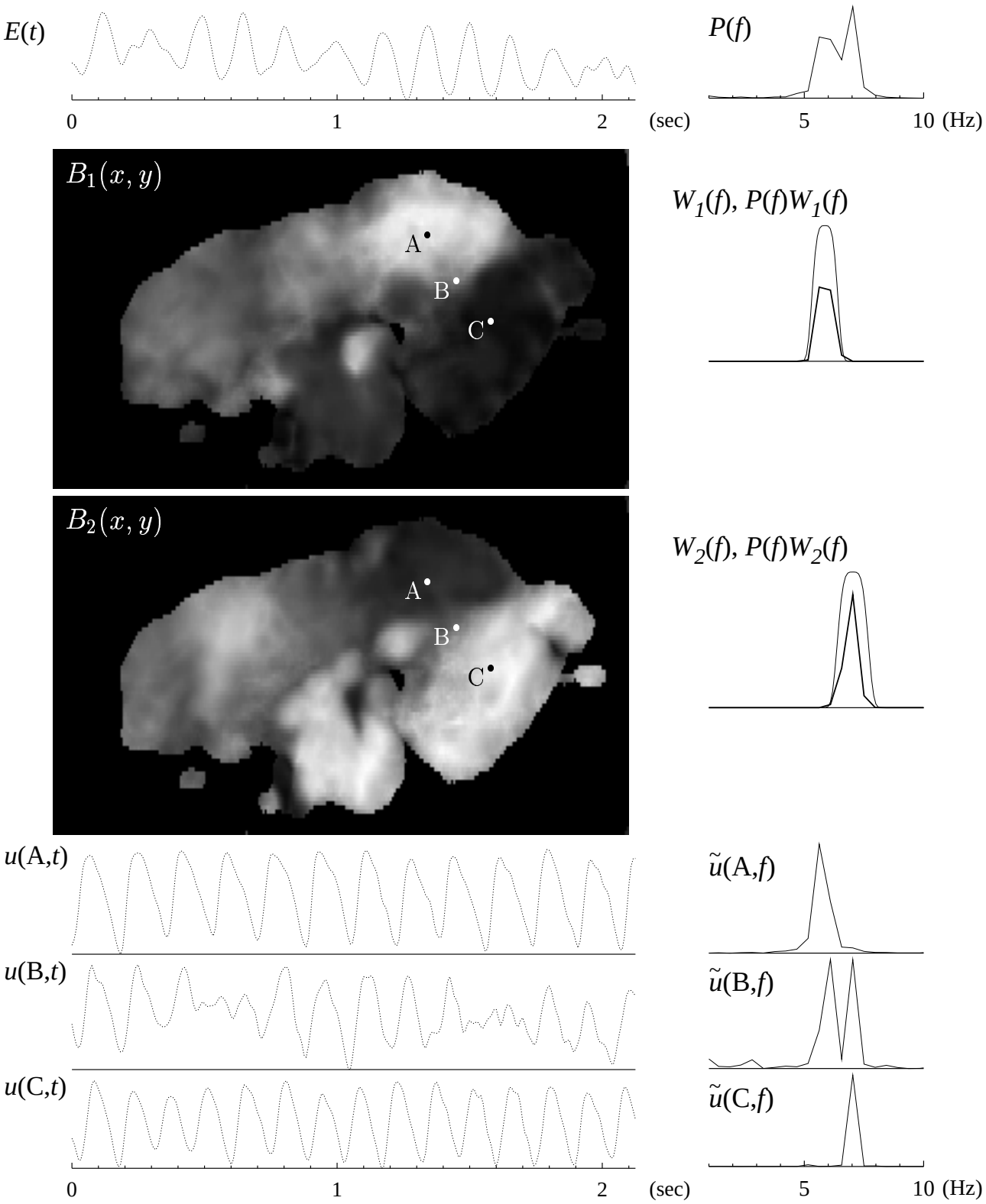

Figure 6: Frequency domains in an experimental polymorphic tachycardia/fibrillation. Top row: pseudo-ECG $E(t)$ (7), and cumulative power spectrum $P(f)$ (9). Below the cumulative spectrum: the filtering windows W_j (thin lines) and cumulative power spectra of the filtered signals PW_j (thick lines). The density plots: frequency domains maps $B_j(x, y)$ (11), the distribution of the power of the frequency bands through the preparation, $j = 1$ (lower frequency) for the upper density plot, abd $j = 2$ (higher frequency) for the lower density plot. Below the density plots: records $u(, t)$ and corresponding power spectra $\tilde{u}(, f)$ at points A, B and C shown on the frequency domains maps. Frequency is in Hz, time is

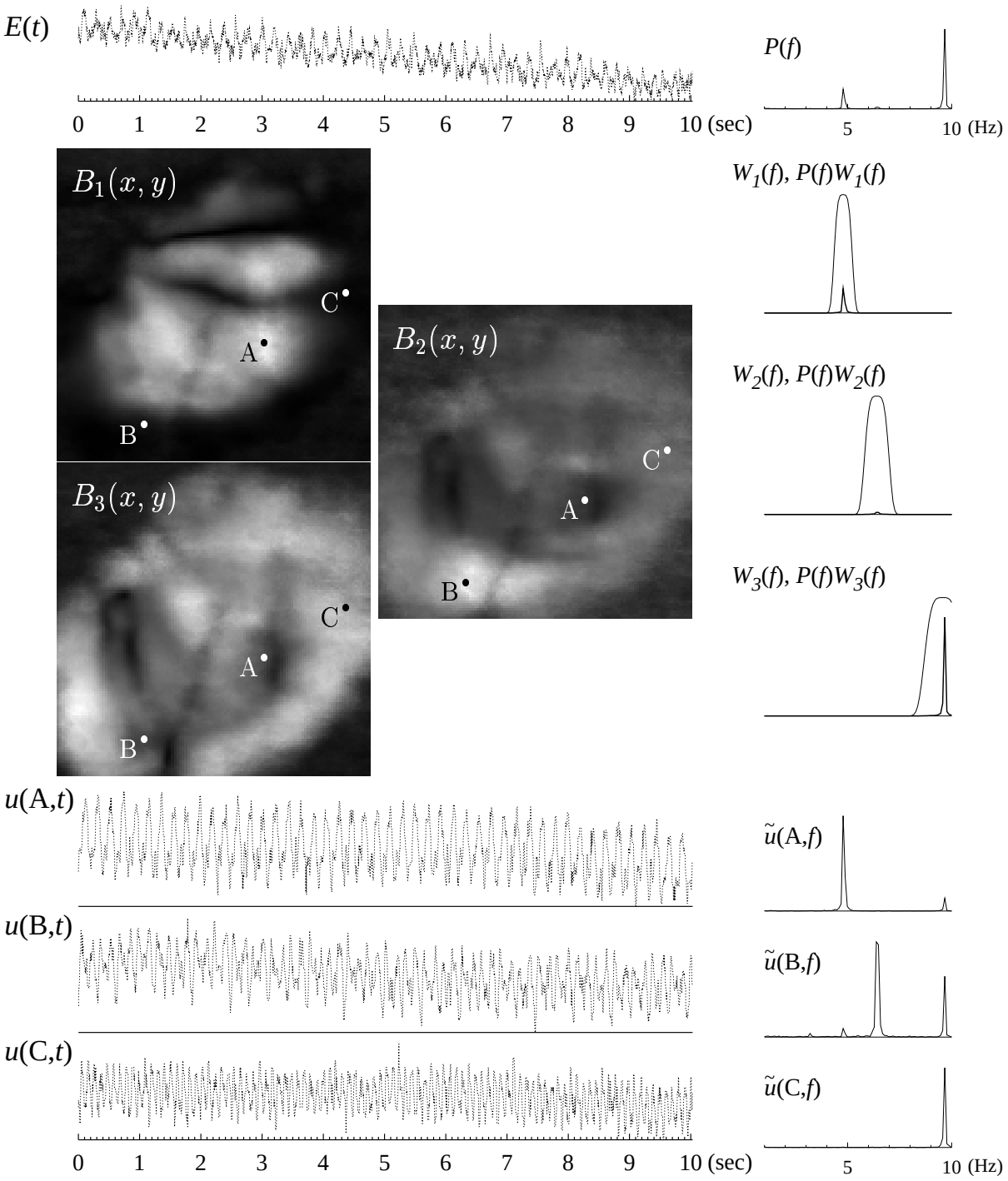

Figure 7: Frequency domain structure in a long-time experimental series with a complicated fibrillatory pattern. Here there are three frequency bands and correspondingly three domain maps; otherwise data format is the same as in Fig. 6.

The power spectra of the signals from different domains domains hardly overlap, the signal from the lower-frequency domains often having a slight high-frequency component, and that the signal from the border zones, as (B) on Fig. 7, has both components. The ratio of the frequencies in Fig. 7 approximately $4:3:2$.

3.2 Simulation: mechanisms of the frequency domain formation

Mechanism M: multiple independent spiral waves. Figure 8 illustrates coexistence of two spiral waves in a model with the stronger inhomogeneity $k = 1.618$. The period of the spiral wave in the right half of the medium is longer than the period in the left half, but no entrainments occur because the waves from the left spiral cannot penetrate the right half as they either come in the excited/refractory phase, or just slightly advance the phase of the right spiral if they come during the excitable gap.

Despite the fact that there are only two stable spiral waves, the pseudo-ECG appears complicated, due to incommensurability of their periods. In order to compare the simulation results with the experiments, we processed the solution $u(x, y, t)$ in the same way as signals from the real experiments. The results are shown on Fig. 9. In this example, as well as in all other numerical data, the frequency peaks were well separated, but higher harmonics present. Often, the second harmonic was more powerful than a main frequency peak. For this reason, visual pre-analysis of spectra was necessary to determine the dominant frequencies.

In the case of Fig. 9, the frequency bands are well separated, both in the frequency domain and in space. There is only a narrow border zone with mixed frequencies. The ratio of the frequencies here was close to the ratio of two small integers, $19.5 : 15 \approx 4 : 3$. Note, however, that the electrograms show no entrainment of one spiral by the other. This is because their cores are sufficiently far from the border separating their domains. In our computation, this independent rotation of spiral waves lasted a very long time. The stability of the spirals was enhanced by presence of inexcitable holes, to which the spiral cores were 'anchored' and did not drift (see [21] for more about anchoring).

Another such example is shown on Figs. 10 and 11, where the ratio of the time constants was less, $k \approx 1.414$. In this case of the lower inhomogeneity, the two spiral waves persisted only for a limited time, about 22 revolutions of the slower spiral and 30 of the faster. After that an excitation wave from the left spiral propagated into the excitable gap of the right spiral, reached its core and pushed it onto the inexcitable boundary. Thereafter, the right part of the medium simply conducted two out of every three excitation waves, *i.e.* the frequency domains were due to the Wenckebach mechanism.

Mechanism W: one spiral wave and Wenckebach frequency division . This mechanism was observed in each of the models described above, by specifying one spiral wave in the faster part of the medium as initial condition. As the period of the spiral in the faster part in both cases is shorter than the refractory period of the slower part, Wenckebach frequency division occured. For model of Fig. 11, that was 2:3, i.e. two out of three waves propagated and every third wave was blocked.

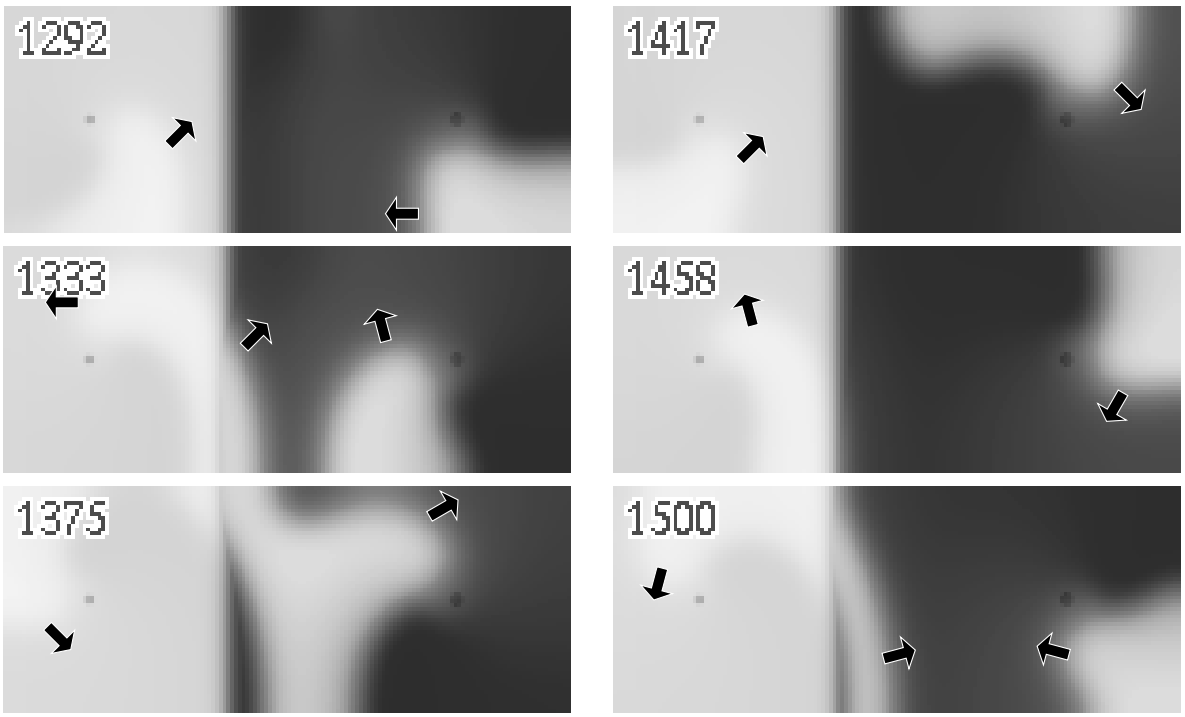

Figure 8: Snapshots of a fibrillatory excitation pattern produced by two spiral waves with incommensurate frequencies, in the numerical experiment. The fast spiral is in the left part of the medium, the slow spiral is in the right part. The background is the distribution of the parameters as on Fig. 2; the excitation wave is shown light upon it. The arrows show the direction of propagation of the waves. Labels show time in milliseconds. Parameters: $k \approx 1.618$, $w = 3$, corresponding to panel (a) of Fig. 2. The thin wave that just entered into the slow right part on panel 1500ms will decay before it meets the wave of the right spiral.

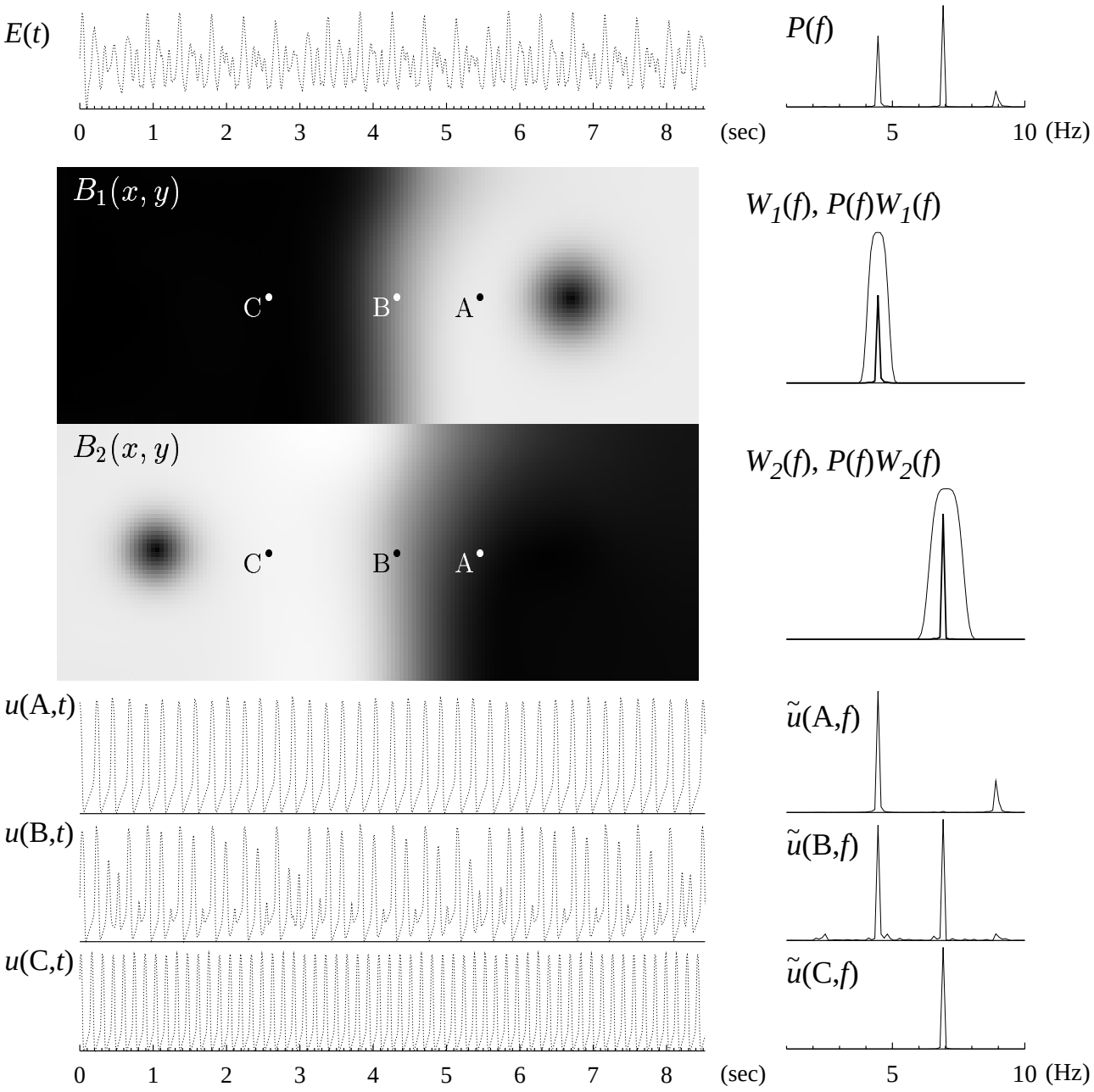

Figure 9: Frequency domain organisation of the numerical fibrillatory pattern shown on Fig. 8. Numerical data processed in the same way as the real experimental data of Figs. 6 and 7.

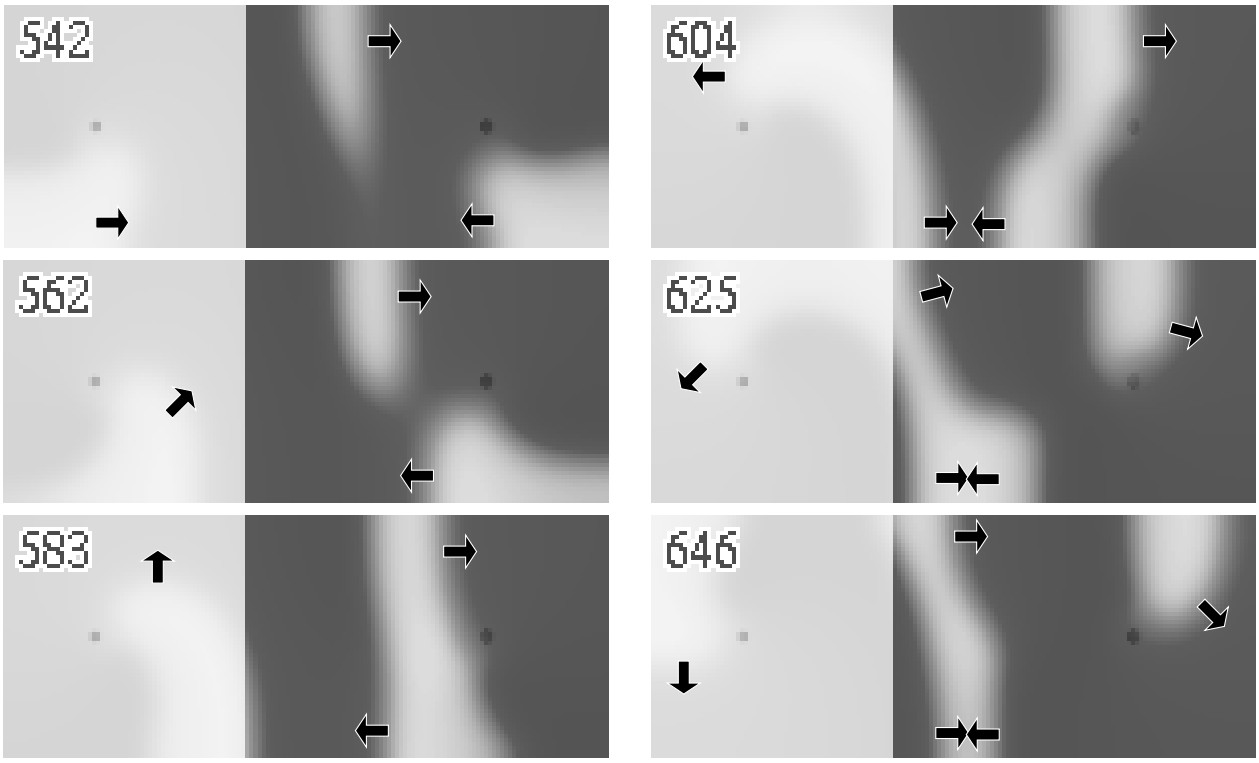

Figure 10: Fibrillatory pattern in a numerical experiment with the weaker inhomogeneity, corresponding to panel (b) of Fig. 2. There are two spiral waves. The faster waves from the left spiral sometimes penetrate to the right part, perturbing the rotation of the slow spiral, as shown on the selected sequence of snapshots; but as the right spiral is pinned to the inhomogeneity, it persists. The slow spiral in the right half existed for 4.2 sec.

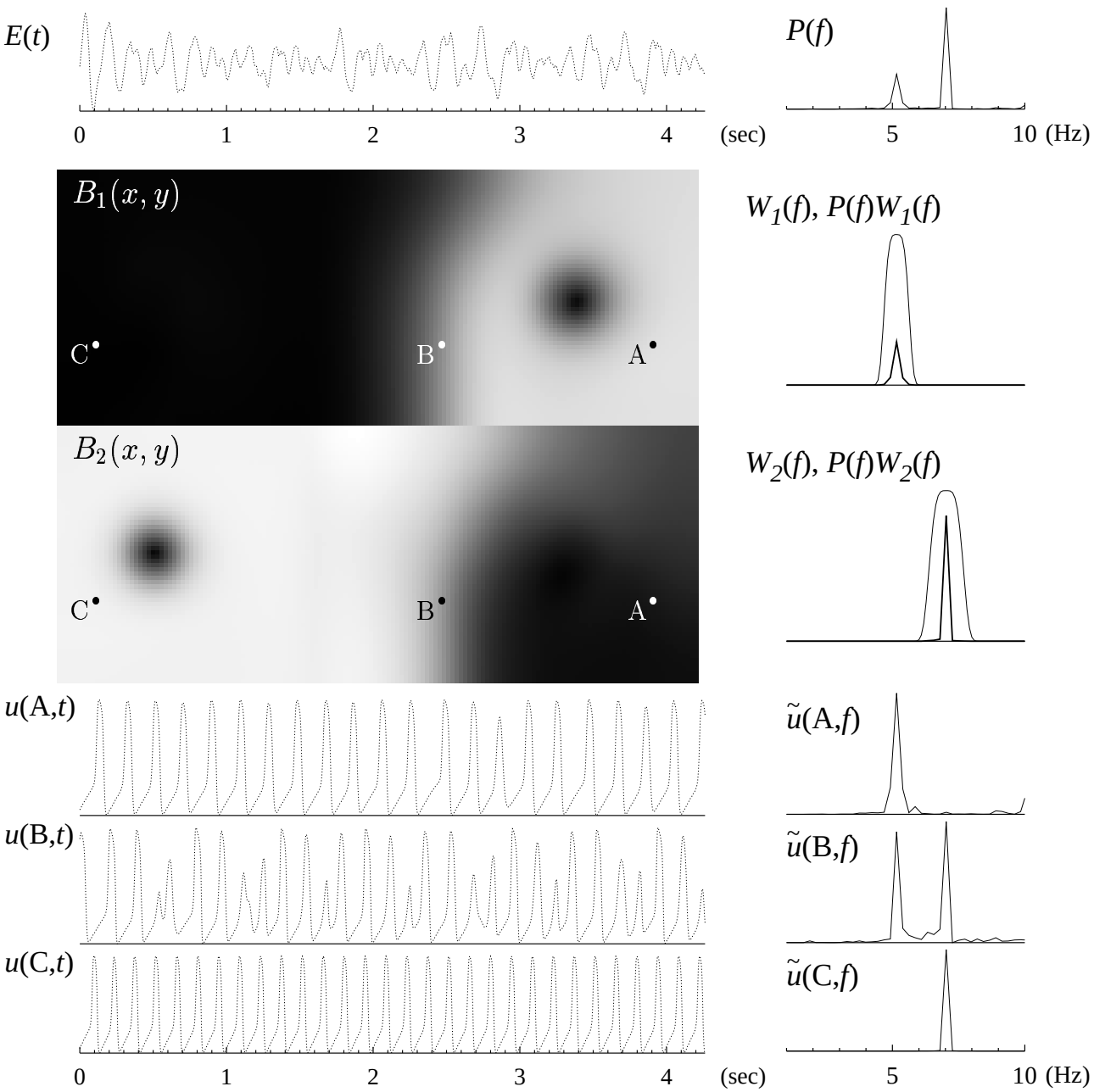

Figure 11: Frequency domain organisation of the pattern of Fig. 8.

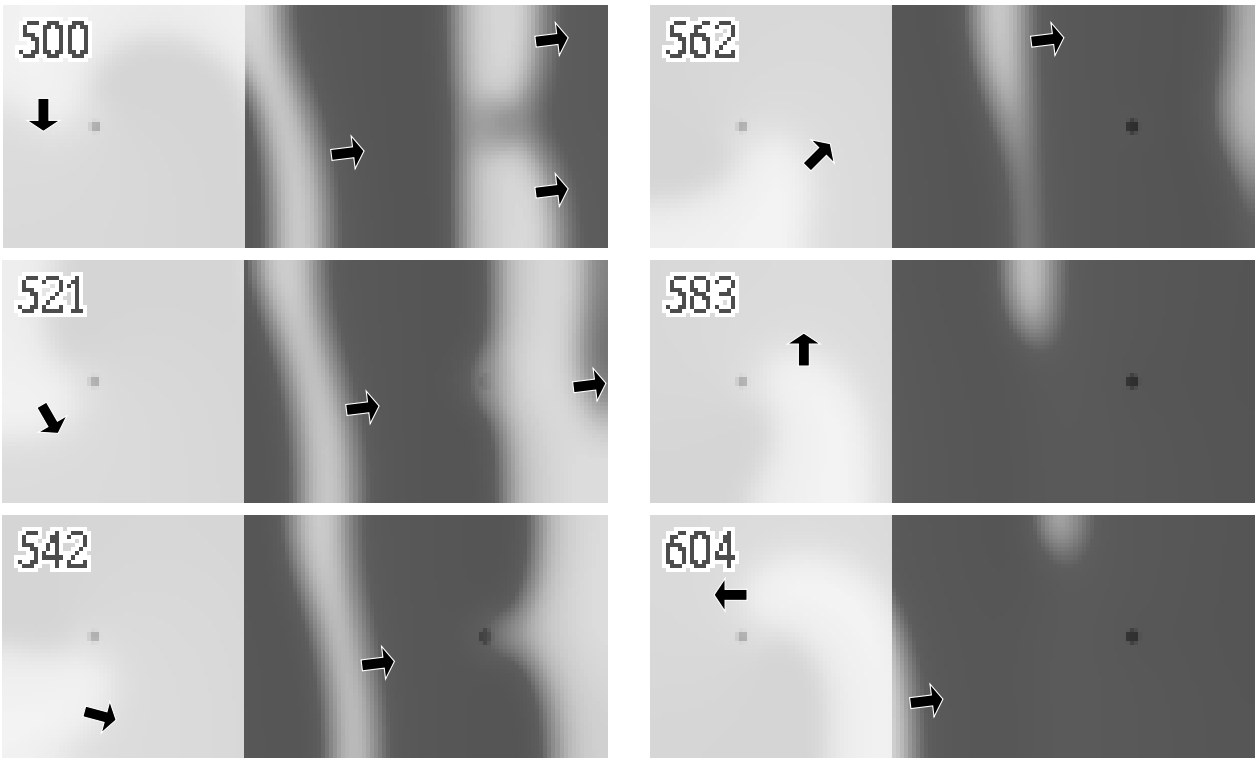

Figure 12: Continuation of the numerical experiment of Fig. 10, 11, after the slow spiral wave in the right part was annihilated. Now the right part is demonstrating 2:3 frequency division. The chosen sequence shows one passed wave and one decayed wave. The time labels are relative to the moment of annihilation of the slow spiral.

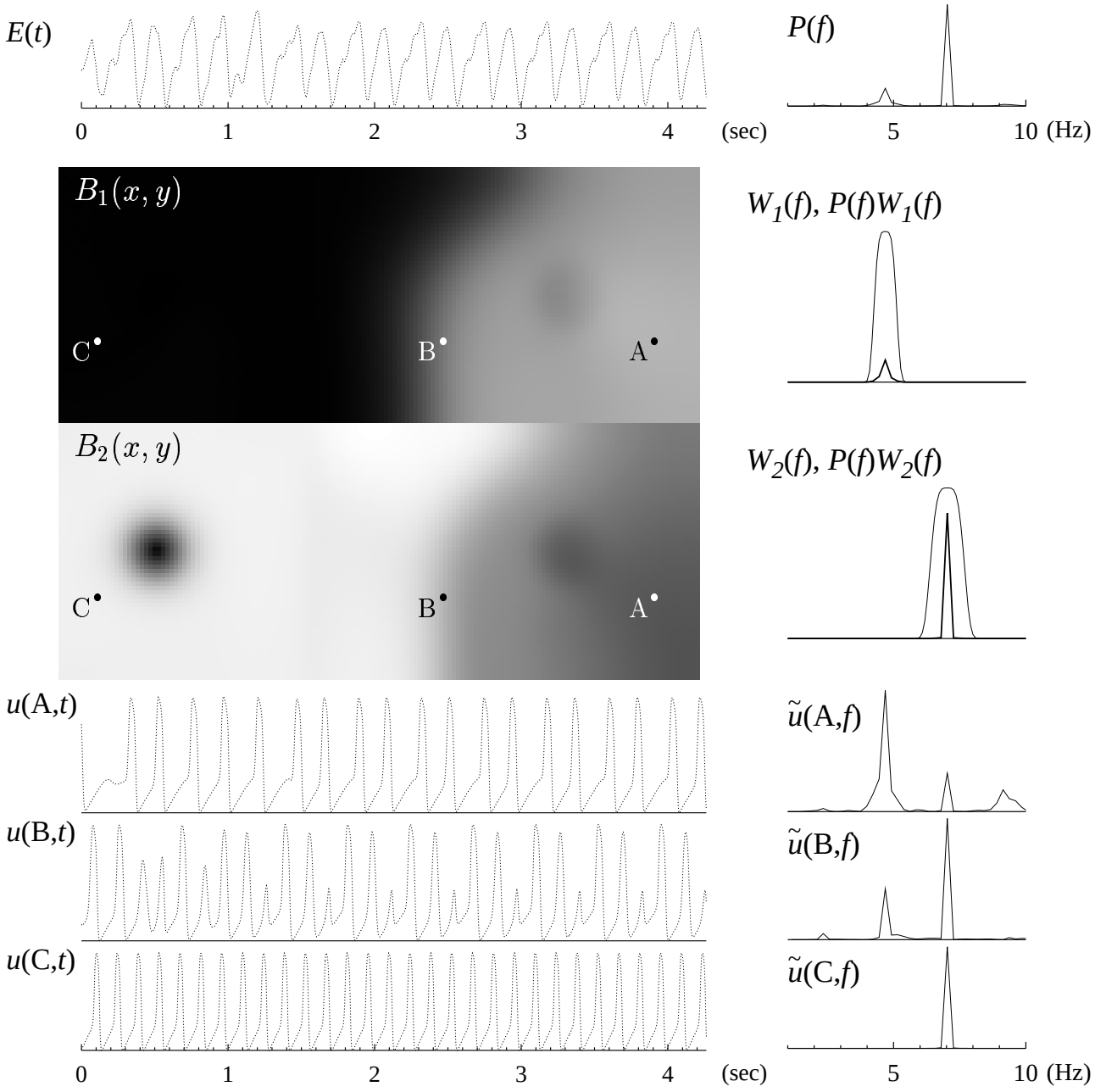

Figure 13: Frequency domain organisation after the annihilation of the slow spiral, corresponding to Fig. 12.

Similar behaviour was observed in the numerical experiment with two spiral waves and $k \approx 1.414$, after the slower spiral terminated. Selected snapshots of the u field are shown on Fig. 12 and corresponding data analysis is given on Fig. 13. It can be seen that the influence of the higher frequency is present in the low-frequency zone, but it diminishes with the distance.

Transition from M to W. Figures 10, 11 and Figs. 12, 13 represent two different mechanisms during different stages of the same numerical experiment. This illustrates the possibility of transition from one mechanism to the other, M to W, and raises the question when such transition can happen. A simple phenomenological criterium can be suggested in the assumption that the core of the slower spiral wave is sufficiently far from the site where the Wenckebach blocks occur. Further into the slower part of the medium from this site, the faster source would appear as a source of modified frequency, *i.e.* frequency divided by the Wenckebach ratio. It is this frequency that will compete with the slower spiral in the slower part of the medium. Therefore, a sufficient condition of the instability of the mechanism M with respect to transition to W is: the Wenckebach-divided frequency of the fast source should be higher than the frequency of the slower source. In other words, the Wenckebach ratio should be lower than the frequency ratio of the two spirals.

As applied to our two numerical experiments, this criterium predicts stability of the slow spirals in both cases. Indeed, in the stronger inhomogeneity of Figs. 8, 9 the spirals' frequency ratio was 1.58 whereas the Wenckebach ratio was found to be 2; and in the weaker inhomogeneity of Figs. 10–13 the spirals's frequency ratio was 1.36 with Wenckebach ratio 1.5.

However, in the second case, Figs. 10 and 12, the slower spiral has been annihilated. This happened because its core was too close to the domain boundary. Thus, in effective prediction of the stability is more difficult, as the above criterium of stability is only necessary but not sufficient. If mechanism M is metastable, its duration may vary greatly.

3.3 Comparative phenomenology of the two mechanisms.

Experimental fibrillation is obviously more complicated process than the numerical mechanisms considered above. This is, in particular, due to such factors as inhomogeneity, anisotropy and three-dimensionality of the real cardiac muscle. This makes the spiral waves invisible or at least unrecognizable on the surface excitation patterns in the majority of cases, and so direct comparison with the two mechanisms is impossible.

There are some robust features of the excitation patterns, however, which would be preserved despite the above mentioned factors; such as e.g. the periods of the re-entry sources. Is it possible to use such features to establish which of the two mechanisms, if any, is responsible for a particular excitation pattern?

In this section, we study some of these features, to see which of them can distinguish between the two mechanisms. These are summarised in the Table 1.

Figure	9	11	13	6
Frequency ratio	1.58	1.36	1.50	1.20
Sharp domain margins present	yes	yes	yes	yes
Broad mixed frequency regions present	no	no	yes	yes
Domains overlap coefficient	0.06	0.11	0.23	0.34
Recurrence seen in the Lissajous curve	no	no	yes	no
Mechanism	M	M	W	M?

Table 1: Diagnostic features of the two mechanisms

Frequency ratio. This is a would-be obvious criterium as for the mechanism W, this ratio must be equal to a ratio of two small integer numbers, whereas for the mechanism M it may be any real number, and therefore if a particular ratio happens to be that of two small integer, it is a strong indication of the Wenckebach mechanism. In practice, however, life is a bit more complicated as the precision with which the frequencies can be determined, is limited by the duration of the signal. For experimental data it is even more difficult as the widths of the frequency peaks are broader and the precision of the main frequencies is less. In the examples considered, frequency ratios of numerical experiments Figures 9 and 11 are significantly different from nearest small-integer ratios, and for Fig. 13 it is exactly 3:2, so in theory this criterium works well. For real experimental data, the ratios are exactly 6:5 for Fig. 6 and very close to 4:3:2 for Fig. 7. This might mean that in both cases mechanism W takes place, or may be a result of a simple coincidence: one can see on these figures that the frequency bands are quite wide for these signals.

Domain boundaries. Figures 11 and 13 are convenient for comparative study of the two mechanisms, as both mechanisms take place in the same 'numerical preparation'. In the two-spiral regime Fig. 11 there is only a thin strip of mixed frequency on the border. In the one-spiral regime, the mixed frequency occupies the major part of the slow half of the medium. This is because the excitation waves propagating through the right part retain the "two passed — one missed" frequency division structure and thus the frequency component of their original source, and the inhomogeneity of their train is only slowly damped down by phase diffusion [25]. Note that in the experimental patterns, see e.g. Fig. 6, thin borders as well as large regions of mixed frequency were observed.

The location and sharpness of the domain borders does not coincide with the borders of the distribution of tissue parameters, which is clearly seen in the numerical experiments. In all four cases, the width of the domain boundary is approximately the same, *i.e.* about 3 space units, whereas the border of the medium parameters was 3 space units wide in one series and 0.2 space units (one computational step) wide in the other series. And in all four cases, the location of the domain borders was significantly displaced with respect to that of medium parameters, into the slower region, so that the domain border and the step in the medium parameters hardly overlap.

To measure the degree of overlap between the domain distributions, we calculated the

overlap coefficient defined as the cosine between these distributions considered as vectors of L_2, i.e.

$$\sigma_{j,k} = \int B_j(x,y)B_k(x,y)\,\mathrm{d}x\,\mathrm{d}y \left(\int B_j(x,y)^2\,\mathrm{d}x\,\mathrm{d}y \int B_k(x,y)^2\,\mathrm{d}x\,\mathrm{d}y \right)^{-1/2} \tag{12}$$

The values of this coefficient are presented in the Table; these agree with the results of visual analysis, i.e. it is larger for the maps where overlap is evident. Its values for the two real experiments are close to each other and are larger than those in numerical experiments. Thus, whereas the overlap coefficient might be a useful diagnostic quantity in principle, it is hardly suitable to reliably distinguish between the two mechanisms.

Lissajous figures. As we already mentioned, closeness of the ratio of the domain frequencies to that of two small integers could be a sign of frequency division, but is not very practical due to the limited length of experimental series and instability of experimental frequencies, seen as large width of the experimental spectra. A classical way to distinguish between commensurate and incommensurate frequency ratios is the Lissajous curve, i.e. the graph of the two signals where the x coordinate is one signal and y coordinate is the other signal. This method, unlike simple numerical comparison of mean frequencies, has the additional advantage that it allows for variations in the signals frequencies as long as these are synchronous. Such variations may widen up the spectra. But the Lissajous figure only monitors the dependence of one signal on the other, and if the frequencies change synchronously then, ideally, the Lissajous figure does not change at all, or realistically, changes only slightly.

Lissajous curves for the numerical experiments described above are presented in Fig. 14.

This was done with filtered signals, computed using forward and inverse Fourier transforms as

$$u_f(x,y,t) = \mathrm{Re}\left(\mathcal{F}^{-1}\left[\tilde{u}(x,y,f) \sum_j W_j(f) \right] \right). \tag{13}$$

where $\tilde{u}(x,u,f)$ is the time-Fourier image (8) of the original signal $u(x,y,t)$, and W_j, $j = 1,2$ are the frequency windows (10).

These Lissajous figures show a clear distinction between the commensurate, (b,d) and incommensurate, (a,c) cases. Disregarding a few loops corresponding to the transient in the beginning of the numerical experiment, panel (b) shows a bold figure which makes 2 up/down motions, e.g. two tops and two bottoms, per one horizontal motion, thus showing 2:1 commensurate frequencies. On panel (d), the transient is more pronounced, so we emphasise the main Lissajous figure showing one complete loop of it with filled circles. This figure has three maxima and minima in the vertical direction vs two maxima and minima in the horizontal direction, thus demonstrating frequency ration 3:2. The panels (a) and (c) do not have such structures and thus demonstrate independent signals.

The Lissajous figures for the tissue experiments shown on Figs. 6 could not be interpreted with such certainty, as their shapes were apparently smeared out by experimental

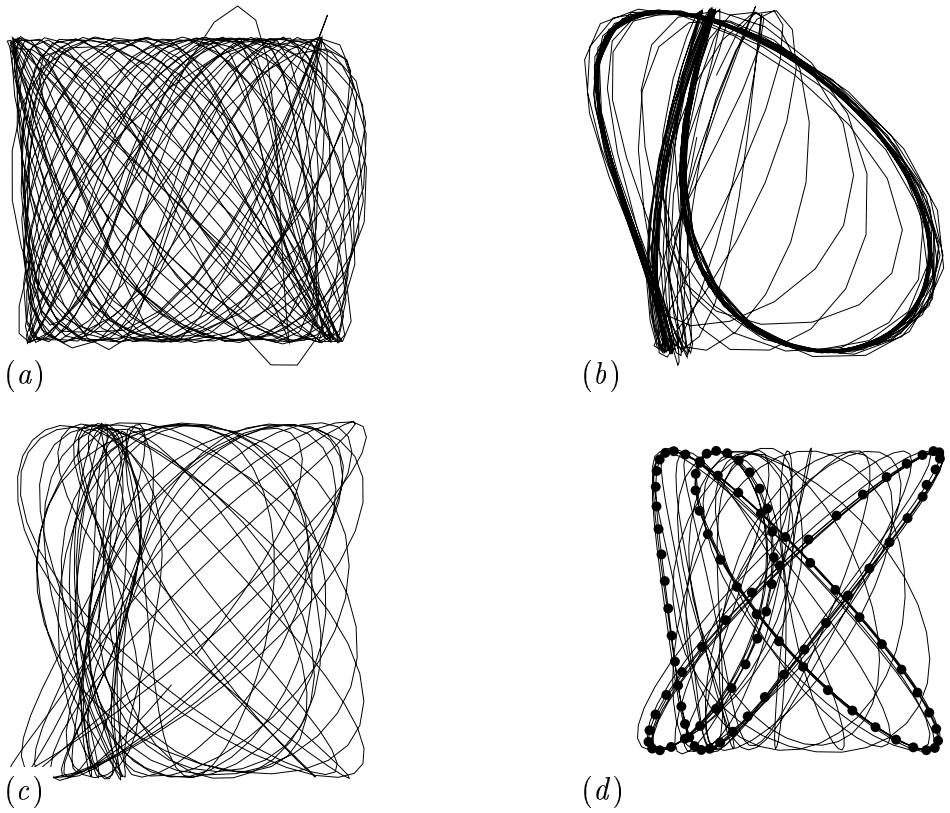

Figure 14: Lissajous curves of numerical experiments: (c) Fig. 9, two spirals, (d) 2:1 Wenckebach mechanism in the same model as Fig. 9, (e) Fig. 11, two spirals, and (f) Fig. 13, 2:3 Wenckebach with a transient. On each graph, the abscissa is record A and the ordinate is record C of the corresponding filtered experimental or numerical series. The filled circles on panel (d) are to emphasise the main Lissajous figure compared to the deviations from it due to the transient.

noise and/or some non-stationary processes in the preparation, which was impossible to establish due to the shortness of the experimental series.

This approach, however, can be quite useful if the experimental data are obtained for a considerably longer time. This is illustrated for the experiment shown on Fig. 7. Figure 15 shows Lissajous figures of signals recorded at the three points A, B, and C in Fig. 7 chosen in three different domains. In this case, the synchronous character of these signals is evident. This figure also illustrates the necessity of the filtering the electrograms, as described in section 2: without such filtering, the synchrony would not be seen. To ensure that this synchrony is not an artifact of the filtering, we plotted similar figures for signals of exactly the same spectra but with randomised phases of the Fourier coefficients. These randomised Lissajous figures are also shown on Fig. 15. They look quite erratic. This proves that the true filtered data show genuine dependence, not reducible to their spectral properties only, and therefore, not due to the filtering. Thus, we can conclude that in this particular experiment, there probably was only one source, with frequency of 9.6 Hz, which was divided in the ratio $2:3$ and $1:2$ in different parts of the preparation.

4 Discussion and Conclusions

Optical monitoring of surface activity is providing high-resolution images of the irregular spatio-temporal activity in different experimental models of ventricular fibrillation [26, 6, 7]. The differences in spatial activity reported here demonstrate the essentially three-dimensional nature of the electrical activity that generates fibrillation in this animal tissue model. Ventricular fibrillation is believed to be produced by re-entrant wave sources, where a single re-entrant source that generates spiral waves in thin, effectively two dimensional tissue, and scroll waves in thicker, three dimensional tissue, breaks down to generate new re-entrant sources. The observed surface patterns of excitation have been interpreted in qualitative terms as the surface manifestations of three-dimensional scroll waves within the ventricular wall [27, 28]. During the course of fibrillation, the number of re-entrant sources increases with time, to fluctuate about some mean. In [27, 28] we have shown that the observed surface patterns of excitation in this preparation can be interpreted in qualitative terms as the surface manifestations of three-dimensional scroll waves within the ventricular wall, with the axis of the scroll filaments lying roughly parallel to the heart surfaces. In an intact heart, these waves would be around filaments which are closed (*i.e.* scroll rings) or that terminate an inexcitable boundary.

The domain structure seen in Figures 1, 2 and 9 is only apparent after Fourier transformation of the signals, and illustrates a local spatial order in the surface activity. The frequency resolution of the Discrete Fourier Transform is limited by the length of the time series analysed, and since fibrillation *in vivo* is a short-lived process the ratio of frequencies obtained from different points will always be between integers. However, the common occurence of simple integer ratios between the dominant frequencies of different domains is highly suggestive of a frequency division mechanism for the domains. The features of most of the tissue experiments can be reproduced by a single re-entrant source, with

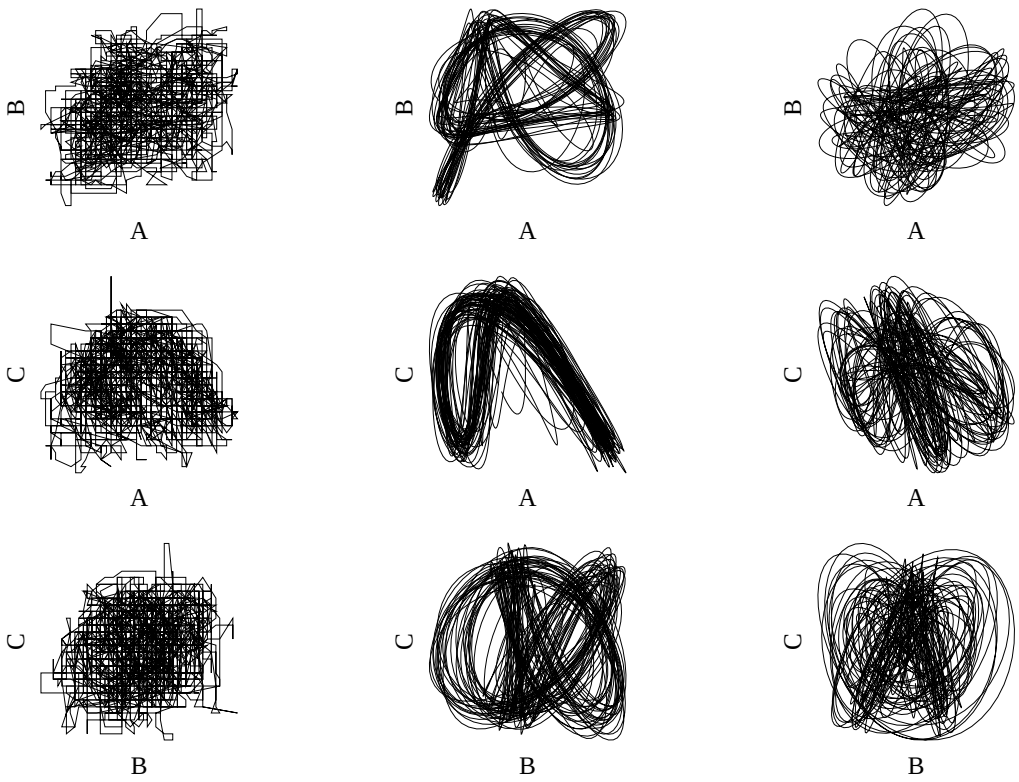

Figure 15: Lissajous figures of the recordings A, B and C of Fig. 7. Left column: raw data. Middle column: filtered data. Right column: filtered data with randomised phases.

intermittent conduction through regions of spatial inhomogeneity producing frequency division; the features of all the tissue experiments can be reproduced by a small number of re-entrant sources and such frequency division. Thus the surface patterns of activity can be reproduced by one, or a few, re-entrant sources, combined with heterogeneity. In the tissue experiments the re-entrant sources will be within the ventricular wall. The ventricular wall has a laminar structure [29], and the connections between neighbouring sheets of ventricular tissue might form the anatomical sites for the heterogeneity that produces the frequency division.

Implications for defibrillation Understanding the detailed processes occuring during actual examples of fibrillation is very important for the design of tools for defibrillation. In particular, the feasibility and realisation of low-voltage defibrillation by feedback driven resonant drift depends on there being only a small number of re-entrant sources [20]. If there is only one re-entrant source, the problem which of the sources to control does not occur. If there are several apparent sources, but these are produced by frequency division from one source, it is necessary to identify that source. For example, for Fig. 7 it is clear that the feedback controlling its motion the should be based on the frequency band of the highest frequency component, that of 9.6 Hz.

Acknowledgements

This work was supported by grants from The Wellcome Trust (045192), EPSRC ANM (GR/L17139), Russian Foundation for Basic Research (96-01-00592) and National Heart and Blood Institute (HL39707).

References

[1] A. V. Holden, M. J. Poole, and J. V. Tucker. An algorithmic model for the mammalian heart: propagation, vulnerability, re-entry and fibrillation. *Int. J. of Bifurcation and Chaos*, 6:1623–1636, 1996.

[2] A. Panfilov and J.P. Keener. Reentry in an anatomical model of the heart. *Chaos Solitons & Fractals*, 5(3–4):681–689, 1995.

[3] R.A. Gray and J. Jalife. Spiral waves and the heart. *Int. J. of Bifurcation and Chaos*, 6(3):415–435, 1996.

[4] A. V. Panfilov. Modelling of re-entrant patterns in an anatomical model of the heart. In A. V. Panfilov and A. V. Holden, editors, *Computational Biology of the Heart*, pages 259–276. Wiley, Chichester, 1997.

[5] O. Berenfeld and J. Jalife. Purkinje-muscle reentry as a mechanism of polymorphic ventricular arrhythmias in a 3-dimensional model of the ventricles. *Circ. Res*, 82:1063–1077, 1998.

[6] R. A. Gray, A. M. Pertsov, and J. Jalife. Spatial and temporal organization during cardiac fibrillation. *Nature*, 392:75–78, 1998.

[7] F. X. Witkowski, L. J. Leon, P. A. Penkoske, W. R. Giles, M. L. Spano, W. L. Ditto, and A. T. Winfree. Spatiotemporal evolution of ventricular fibrillation. *Nature*, 392:78–82, 1998.

[8] V. N. Biktashev, A. V. Holden, S. F. Mironov, A. V. Zaitsev, and A. M. Pertsov. Intermittent conduction block can account for the spatial distribution of dominant frequencies during ventricular fibrillation. *J. Physiol.*, 518P:P38, 1999.

[9] A. V. Zaitsev, O. Berenfeld, J. Jalife, S. F. Mironov, and A. M. Pertsov. Distribution of excitation frequencies on the epicardial and endocardial surfaces of fibrillating ventricular walls of the sheep heart. *Circ. Res.*, 86(4):408–417, 2000.

[10] Denis Noble. *Oxsoft HEART Version 3.8 manual.* Oxsoft, Oxford, 1990.

[11] Vadim N. Biktashev and Arun V. Holden. Re-entrant activity and its control in a model of mammalian ventricular tissue. *Proc. Roy. Soc. Lond. ser. B*, 263:1373–1382, 1996.

[12] Alexander V. Panfilov and James P. Keener. Reentry in 3-dimensional FitzHugh-Nagumo medium with rotational anisotropy. *Physica D*, 84(3–4):545–552, 1995.

[13] F. Fenton and A. Karma. Fiber rotation induced vortex turbulence in thick myocardium. *Phys. Rev. Lett.*, 81:481–484, 1998.

[14] Vadim N. Biktashev, Arun V. Holden, and Henggui Zhang. Tension of organizing filaments of scroll waves. *Phil. Trans. Roy. Soc. Lond. ser. A*, 347:611–630, 1994.

[15] Vadim N. Biktashev. A three-dimensional autowave turbulence. *Int. J. of Bifurcation and Chaos*, 8(4):to appear, 1998.

[16] A. T. Winfree. Electrical turbulence in 3-dimensional heart muscle. *Science*, 266(5187):1003–1006, 1994.

[17] F. Xie, Z. Qu, J. N. Weiss, and A. Garfinkel. Interactions between stable spiral waves with different frequencies in cardiac tissue. *Phys. Rev. E*, 59:2203–2205, 1999.

[18] A.M. Pertsov and E.A. Ermakova. Mechanism of the drift of a spiral wave in an inhomogeneous medium. *Biofizika*, 33(2):338–342, 1988. in Russian.

[19] V. G. Fast and A. M. Pertsov. Drift of vortex in myocardium. *Biofizika*, 35(3):478–482, 1990. in Russian.

[20] V. N. Biktashev and A. V. Holden. Resonant drift of autowave vortices in 2D and the effects of boundaries and inhomogeneities. *Chaos Solitons & Fractals*, 5(3,4):575–622, 1995.

[21] M. Vinson, A. Pertsov, and J. Jalife. Anchoring of vortex filaments in 3D excitable media. *Physica D*, 72(1–2):119–134, 1994.

[22] A. M. Pertsov, C. Cabo, W. T. Baxter, R. A. Gray, J. M. Davidenko, and J. Jalife. Thinning of the myocardial wall as an attractor of vortex-like reentry in a 3-dimensional model of cardiac excitation. *Circulation*, 90(4 Pt2):519, 1994.

[23] A. M. Pertsov, J. M. Davidenko, R. Salomonsz, W. Baxter, and J. Jalife. Spiral waves of excitation underlie reentrant activity in isolated cardiac muscle. *Circ. Res.*, 73(3):631–650, 1993.

[24] V. Krinsky, A. Pertsov, V. Fast, and V. Biktashev. A study of autowave mechanaisms of cardiac arryhthmias. In A. V. Holden, M. Markus, and H. G. Othmer, editors, *Nonlinear Wave Processes in Excitable Media*, pages 5–13. Plenum, New York, 1991.

[25] V. N. Biktashev. Diffusion of autowaves. Evolution equation for slowly varying autowaves. *Physica D*, 40(1):83–90, 1989.

[26] A. V. Holden. Cardiac physiology - a last wave from the dying heart. *Nature*, 392:20–21, 1998.

[27] V. N. Biktashev, A. V. Holden, S. F. Mironov, A. M. Pertsov, and A. V. Zaitsev. Three dimensional aspects of re-entry in two models of ventricular fibrillation. *J. Physiol.*, 509P(SISI):P139, 1998.

[28] V. N. Biktashev, A. V. Holden, S. F. Mironov, A.M. Pertsov, and A.V. Zaitsev. Three dimensional aspects of re-entry in experimental and numerical models of ventricular fibrillation. *Int. J. of Bifurcation and Chaos*, 9(4):694–704, 1999.

[29] I. J. LeGrice, B. H. Smaill, L. Z. Chai, S. G. Edgar, J. B. Gavin, and P. J. Hunter. Laminar structure of the heart — ventricular myocyte arrangement and connective tissue architecture in the dog. *American Journal of Physiology — Heart and Circulatory Physiology*, 38(2):H571–H582, 1995.